Total Ionizing Dose, Random Dopant Fluctuations, and its combined effect in the 45 nm PDSOI node

Eleni Chatzikyriakou, William Redman-White, C.H. De Groot

Department of Electrical and Computer Science, University of Southampton

Abstract

Total Ionizing Dose and Random Dopant Fluctuation simulations in 45 nm Partially Depleted Silicon-on-Insulator nMOSFETs are presented. Calibration is done according to the commercial IBM 45 nm technology node. The importance of the bottom corner parasitic transistor to the Total Ionizing Dose response is shown with the use of ultra shallow junctions. Simulation of irradiation in two-dimensional slices of the device reveal that the majority of the charge is trapped around the silicon film and at the bottom of the Buried OXide in the case of a positive gate bias. Random Dopant Fluctuations are examined using the Sano and the Impedance Field Method. The simulation results of the two methods are in good agreement. Dopant fluctuations do not produce significant response variation pre-irradiation, but they affect post-irradiation results introducing statistical deviations and aggravating Total Ionizing Dose effects. This effect is more pronounced during weak inversion of the parasitic transistor.

Keywords:
Simulation, Finite Elements Method, Total Ionizing Dose, Partially Depleted, Silicon-on-Insulator, Random Dopant Fluctuations

1. Introduction

Partially-Depleted Silicon-on-Insulator (PDSOI) nMOSFETs of sub-100 nm gate lengths have been shown to exhibit increased hardness against Total Ionizing Dose (TID) due to the high body doping incorporated to suppress short channel effects [1, 2] and the use of a thick silicon film that mitigates electrostatic coupling between the front gate transistor and any parasitic channels induced in the device after irradiation [3]. Furthermore, the Buried OXide (BOX) insulates the active silicon region from charge collected in the bulk making them less susceptible to Single Event Effects [4]. To this end, the 45 nm commercial SOI node is a good candidate for aerospace and aviation applications.

TID-induced degradation in these devices is manifested as increase in the off-state current (I_{off}) that results from the formation of parasitic transistors at the sidewall of the active silicon region adjacent to the Shallow Trench Isolation (STI) and at the back interface of the top silicon layer with the BOX [5–10]. Threshold voltage shifts induced by gate oxide charge are less pronounced due to the increased probability of the charges tunnelling out of these thin oxides [11–14].

Variations in the TID response of bulk sub-100nm MOSFETs such as that caused by STI topology and stress have been studied previously [15, 16] on the premise that identical devices from the same lot have exhibited similar pre-irradiation and different post-irradiation response [17]. In this work, Random Dopant Fluctuations (RDF) arising as a result of the low total number of dopant atoms implanted in the small volume of the active silicon region, are examined. The commercial simulation software Synopsys Sentaurus is used for this purpose.

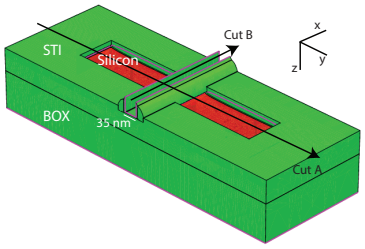

(a) 3D structure

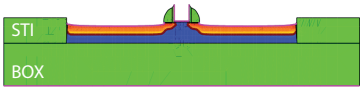

(b) Cut A

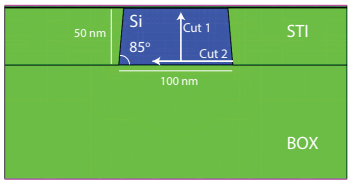

(c) Cut B

Figure 1: 45 nm PDSOI MOSFET simulation model. (a) 3D structure (b) 2D cut A (c) 2D cut B

RDFs as a source of variability become significant in deca-nanometer technologies. It has been suggested that at 45 nm

Email address: ec3g12@soton.ac.uk (Eleni Chatzikyriakou)

	IBM 45 nm node	This work
Physical L_g (nm)	35	35
EOT (nm)	1.0	1.0
t_{Si} (nm)	60	50
I_{dSat}(μA/μm)	1240	1220
I_{off} (nA/μm)	200	4
V_t (V)	0.35	0.36
V_{dd} (V)	1.0	1.0

Table 1: 45 nm device characteristics as measured experimentally [20] and simulated (this work).

they approach 50% of total variability [18]. In [19], it is shown that random discrete dopants can have a significant effect in device response when also taking into account traps located at the channel region and created due to device degradation. Our current focus is on the effects that changes in the number and position of dopant atoms can have on the TID response of the device taking into account that such effects require a large number of devices to be measured. Furthermore, using simulation tools, the variations due to RDFs can be measured separately from other variation sources.

2. Simulation details

A floating body 45 nm PDSOI nMOSFET was constructed in Sentaurus process (Figure 1). The steps are similar to the gate-first flow in [22]. Important device characteristics and structural parameters are shown in conjunction with those in [20] and [23] in Table 1. I_d-V_g results of the simulation are compared to the experimental results from [21] in Figure 2.The doping profile in two directions inside the silicon film is shown in Figure 3. The doping level in the device is between 3×10^{18} cm^{-3} and 5.4×10^{18} cm^{-3}. The doping profile is constant in the third dimension as our device was first created in 2D and then extruded to 3D. This assured that the same doping level extends to the STI sidewalls.

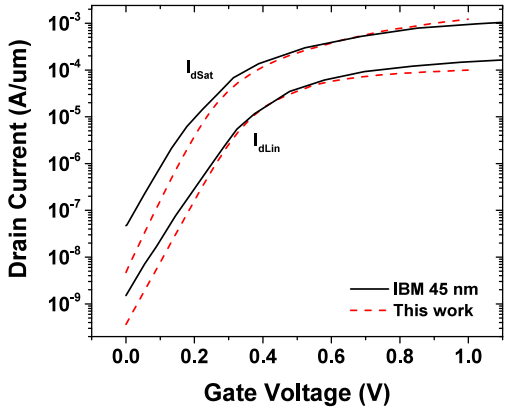

Figure 2: I_d-V_g simulation results of 45 nm PDSOI MOSFET compared to experimental results from [21]

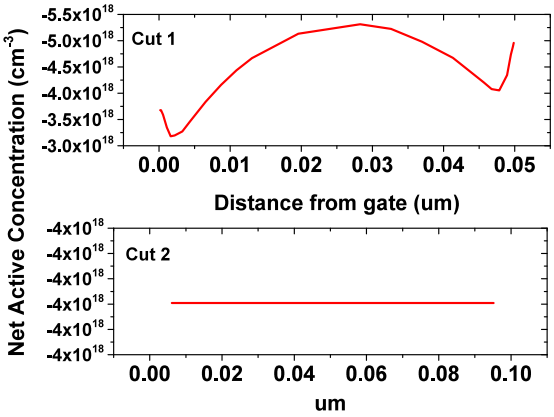

Figure 3: Doping concentration through Cut 1 and 2 as shown in Figure 1c.

The oxide regions surrounding the device are separated, so that contributions from the STI and BOX can be examined separately. The thickness of the BOX and STI is 100 nm following previous studies showing that charge is collected up to this distance from the interface with the silicon [24].

The topology of the device at the corners created by the isolation oxides is very important to the device response [25]. The 'humps' observed in I_d-V_g results in earlier technologies were caused by charges gathering at the top silicon/STI corner when the trench is recessed [26]. Other authors indicate the absence of humps in certain technologies [27, 28] and its correlation to simulation results with fixed oxide charges. It is generally concluded that humps are observed in situations where the top STI corner is not sufficiently rounded and irradiation occurs under zero bias, as positive gate voltages push holes towards the bottom of the STI. In this work, we have used a planar STI configuration in order to examine the effects of RDFs on the sidewall channel excluding topology effects.

The 'back' and 'sidewall' electron routes inside the device seem less favorable over that at the bottom STI corner for PDSOI structures. In [28], an analytical expression is derived for inversion of this corner parasitic transistor. The device sidewall angle used in the simulations is 85^o, which is an approximate value commonly encountered in the technology of interest [29, 30]. Furthermore, to investigate the case where no contact of the Source/Drain regions to the BOX occurs, ultra-shallow junctions of x_j = 20 nm were used.

Electron transport in the silicon region directly below the gate is simulated using the hydrodynamic model. The Philips Unified Mobility model is included with degradation due to the electric field perpendicular to the silicon/SiO_2 interface. The physical thickness of the gate oxides is 0.8 nm for SiO_2 and 1.5 nm for HfO_2.

3. Uniform profile results

3.1. Fixed oxide charge

Initially, the devices were solved with uniform bulk fixed oxide charges and a uniform doping profile. The I_d-V_g results for

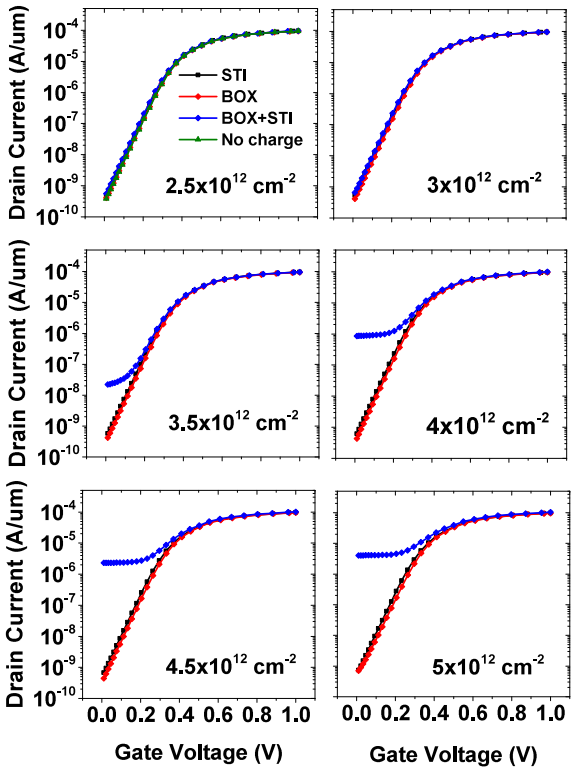

Figure 4: I_d-V_g results of 45nm PDSOI with uniform doping profile and uniform bulk field oxide charges

different densities of charge trapped in the BOX, the STI and both the BOX and STI are shown in Figure 4. These results are similar to another 45 nm technology examined both computationally and experimentally in [31].

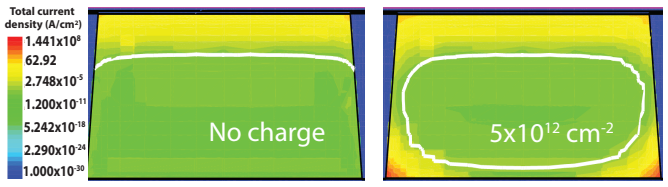

Figure 5: Depletion region width and off-state current density at V_g=0 V, V_{ds}=0.05 V through Cut B of Fig. 1. The white line indicates the boundaries of the depletion region.

Specifically, the increased areal charge required to invert the parasitic channel is attributed to the high body doping we have used in our technology calibration and the distribution of the doping profile in the device. For the BOX only case, very minimal conduction of the parasitic structure is observed at 5×10^{12} cm^{-2}, while the threshold voltage shift observed for this structure due to STI charge of the same density is 10 mV. It is clear that even though the S/D implants do not extend to the BOX, radiation affects off-state current significantly. This, however, only happens when both the BOX and STI charges are included. The width of the depletion regions and the current density is shown in figure 5 for the cases of no charge and uniform oxide charge of 5×10^{12} cm^{-2}. The location of the parasitic inversion charge occurs mainly at the bottom silicon corner, with the holes trapped in the field oxides acting as lateral gates in the top silicon film.

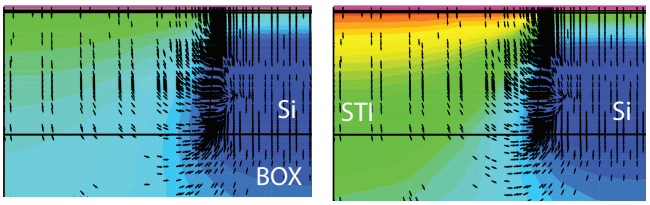

(a) V_g = 0 V, V_{ds} = 0.05 V (b) V_g = 1 V, V_{ds} = 0.05 V

Figure 6: Electric field lines in the field in the three-dimensional 45 nm PDSOI MOSFET model. The coloured gradient shows the electrostatic potential

Figure 6 shows the electric field lines in the field oxides. Their direction further confirms that the bottom corner transistor takes place in our device. Holes created in the STI and BOX follow the direction of the electric field lines and get trapped in defect centers (E_γ' and E_δ') [32]. According to the theory, the trapped charge density will be higher towards the end of the lines at the interface with the silicon, as the hole flux there will be higher. Ionic hydrogen (H^+) originating from the oxide also follows the same path. At the Si/SiO_2 interface, hydrogen can de-passivate dangling bonds creating either interface traps, or introducing fixed positive charge [33]. In our device, the field lines have a similar distribution as that in over-etched STI 0.2 μm PDSOI MOSFETs [28], moving from the STI to the BOX and from the BOX towards the silicon and the bottom silicon corner [34].

3.2. Radiation simulations

Radiation simulations were further performed in a two-dimensional cut of the PDSOI structure in order to quantify the amount of bulk charge trapped in the BOX and STI as well as its distribution. The radiation generation model of Sentaurus device was used for this purpose, which has been well-calibrated previously in [35, 36]. Drift-diffusion was used for the transport of the carriers in the oxide. Hydrodynamic transport is disabled for both the silicon and the oxide. The simulation parameters used for the carrier generation, transport and trapping are shown in Table 2 [12, 35]. Holes are assumed to be trapped in defects (E_γ' and E_δ' centers) in the field oxides.

Donor traps with uniform concentration and a deep effective activation energy of 4 eV above the valence band, representing deep traps that remained filled the longest after irradiation are assumed. For trapping, the drift motion of the carriers is fully taken into account, and diffusion is completely neglected. For both electrons and holes, the degeneracy factor of the gap energy states is unity and the constant emission rate is zero.

The 2D cut is taken as shown in Figure 1c. The contact of the oxide with the metal gate is defined as Schottky. The bottom of the BOX has a silicon region adjacent to it. A substrate bias is applied to fix the electrostatic potential to that of the three

Irradiation term	g	$7.6{\cdot}10^{12}$	$cm^{-3}Rad(SiO_2)$
Dose Rate	$\dot{D}$	38.6	$Rad(SiO_2)/s$
Electron Mobility	μ_n	20	$cm^2\ V^{-1}\ s^{-1}$
Hole Mobility	μ_p	10^{-5}	$cm^2\ V^{-1}\ s^{-1}$
Electron thermal velocity	v_{th}^n	2.042×10^7	cm/s
Hole thermal velocity	v_{th}^p	1.562×10^7	cm/s
Electron capture cross section	σ_n	10^{-12}	cm^2
Hole capture cross section	σ_p	$6.8{\times}10^{-14}$	cm^2
Effective density of states in conduction band	N_C	$8.867{\times}10^{18}$	cm^{-3}
Effective density of states in valence band	N_V	$1.931{\times}10^{20}$	cm^{-3}
Energy of donor traps	E_{trap}	$E_V{+}4$	eV
Donor traps density	p_t	$5{\times}10^{18}$	cm^{-3}

Table 2: Parameters used for radiation simulations

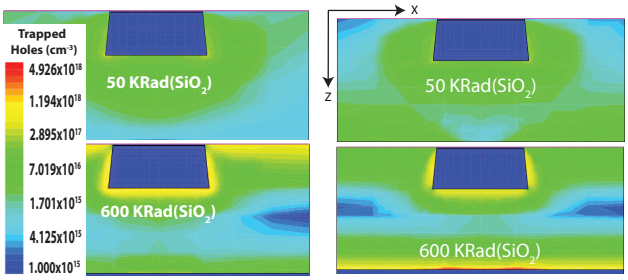

(a) V_g = 0 V (b) V_g = 1 V

Figure 7: 2D simulation results of positive trapped charge density in the STI and BOX (cm^{-3}). The cut is taken in the direction as shown in Figure 1c.

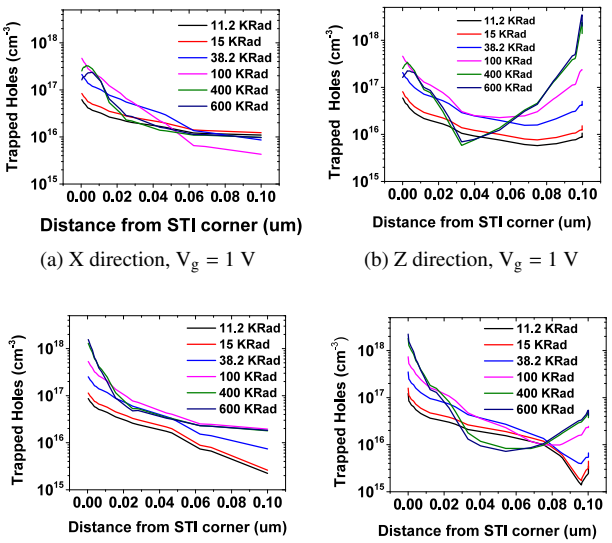

(a) X direction, V_g = 1 V (b) Z direction, V_g = 1 V

(c) X direction, V_g = 0 V (d) Z direction, V_g = 0 V

Figure 8: Trapped charge as a function of distance from the bottom silicon corner

dimensional model used for the RDF simulations. Thermionic emission is enabled between the silicon region and the oxide. Generated carriers are able to leave the oxide both through the gate and with the process of thermionic emission towards the silicon.

The 2D simulation results under two different bias conditions (V_g = 0 V and V_g = 1 V) are shown in Figure 7. The highest density of the trapped charge is aggregated around the silicon film. At V_g = 1 V, the trapped charge density is increased at the bottom of the BOX as well, as the holes are pushed towards it by the positive gate bias. This reduces the amount of holes trapped underneath the silicon film with increasing radiation, a process that is also dependent on the annealing time of the positive trapped charge.

Trapped charge as a function of distance from the bottom silicon corner for both bias conditions is shown in Figure 8. At V_g = 1 V, the high density of trapped holes at the bottom of the BOX is observed more clearly (Figure 8b). There exists a peak of trapped charge concentration at the bottom silicon corner at 100 $KRad(SiO_2)$. Beyond that, the density starts decreasing under the influence of the holes trapped at the bottom of the BOX. Charge is then pushed to the STI sidewalls. Similarly, the charge trapped at the bottom of the silicon film at V_g = 0 V is affected by the charge trapped at the bottom of the BOX (Figure 8d). In this case, holes are pushed towards the substrate under the influence of the positive charge trapped at the bottom of the silicon film. In both cases, the electric field is reduced in the middle of the BOX between the two interfaces with the silicon, causing less electron-hole pairs to be generated, a process described as 'electric field collapse' [37].

The highest value of areal trapped charge at the bottom of the silicon corner for V_g = 0 V occurs above 400 $KRad(SiO_2)$ with $9.4{\times}10^{11}$ cm^{-2} in the X direction and $7.5{\times}10^{11}$ cm^{-2} in the Z direction. At V_g = 1 V, the highest areal trapped charge density is at 300 $KRad(SiO_2)$ with $5.6{\times}10^{11}$ cm^{-2} in the X direction and $4.3{\times}10^{11}$ cm^{-2} in the Z direction. All values are below the value required for parasitic channel inversion, as was shown in the fixed charge simulations, indicating that a higher density of traps would be needed to reach inversion of the parasitic transistor.

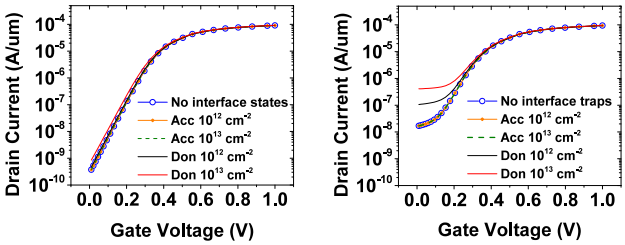

(a) No bulk oxide charge

(b) Fixed bulk oxide charge N_{ot} = 3.5×10^{12} cm^{-2}

Figure 9: I_d-V_g results of the 45 nm PDSOI MOSFET with and without bulk fixed oxide charge and interface traps.

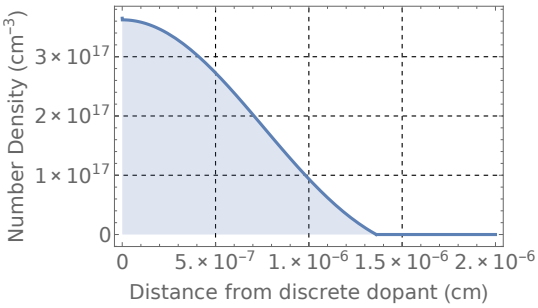

Figure 10: Number density of the dopant atom as a function of distance from its center with screening length 3 nm

3.3. *Interface traps*

To examine the effects of traps located at the interface of the BOX and STI with the top silicon film, the simulations shown in Figure 9 were performed. Donor and acceptor interface traps were examined separately with areal concentrations up to 10^{13} cm^{-2}. The activation energies of the traps are 0.45 eV from the silicon conduction band for the acceptors traps and 0.45 eV from the valence band for the donor traps, that represent the worst case scenario.

Acceptor traps remained unoccupied based on the electrostatic potential at the Si/SiO_2 interface. Donor traps with concentration of 10^{13} cm^{-2} created a V_t shift of 12 mV and ΔI_{off} = 1.82×10^{-10} A/μm in the case where no bulk charge (N_{ot}) was considered. Under weak inversion of the parasitic transistor (N_{ot} = 3.5×10^{12} cm^{-2}), further increase of leakage current when compared to the device with bulk oxide charge, ΔI_{off} = 3.93×10^{-10} A/μm, was observed.

The net effect of donor interface traps when combined with bulk oxide charge is a negative threshold voltage shift of the parasitic transistor. Leakage current is therefore observed in lower values of bulk oxide charge.

4. Random Dopant Fluctuations

Two different methods were used for the RDF simulations: The Sano method and the Impedance Field Method (IFM). Uniform fixed oxide charge was used in both cases.

4.1. *Sano Method*

Using the Sano method in Sentaurus mesh, the doping concentration in the device is first translated to a total number of atoms, then, both their number and position is randomized and re-assigned to the mesh. The number density of the discrete dopant is given by the long range part of the Coulomb potential,

$$n(r) = \frac{k_c^3}{2\pi^2}\frac{sin(k_c r) - (k_c r)\,cos(k_c r)}{(k_c r)^3} \qquad (1)$$

where k_c is the screening factor and r is the distance from the atom. One method of calculating the screening length is the Conwell-Weisskopf model [38, 39] defined as,

$$\frac{1}{k_c} \approx \frac{1}{2\times N_{ac}^{1/3}} = 3\times10^{-7} cm \qquad (2)$$

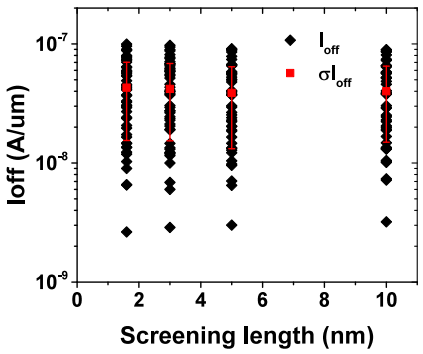

Figure 11: Effects of screening length on I_{off} values.

for doping density N_{ac} = 4.6×10^{18} cm^{-3} extracted from the simulator. In Sentaurus mesh, the oscillatory function is cut-off at the first occurrence of zero. The normalized doping density as a function of distance from the atom is shown in Figure 10. Simulations were performed to test the effects of the screening length on the spread of I_{off}. This is shown in Figure 11. σI_{off} showed negligible change in a screening length range of 1.5 nm to 10 nm. Therefore, the Conwell-Weisskopf model can be safely used.

Only the silicon volume directly underneath the gate was randomized (Figure 12). The total number of atoms encountered in the randomized profile devices had a range of 544 - 700. The frequency distribution of devices with dopant atoms within a specific range is shown in Figure 13. For 100 samples that were produced, the mean is just above the nominal device which has 600 atoms. There is also a tail towards the maximum.

I_d-V_g results of the devices with the randomized doping profiles for the cases of combined BOX and STI charge are shown in Figure 14. It is observed that the spread in I_{off} is higher at 3.5×10^{12} cm^{-2}. At this areal charge, the parasitic transistor is at the point of weak inversion. Beyond that, the parasitic transistor is completely turned on and the spread reduces to its minimum.

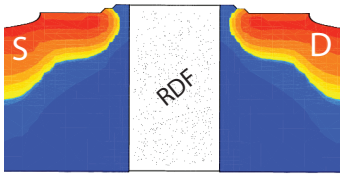

Figure 12: Active silicon region where RDFs are applied

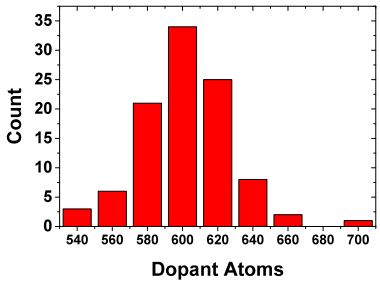

Figure 13: Frequencies of devices with total number of atoms in the region where randomization was performed as labelled in X axis

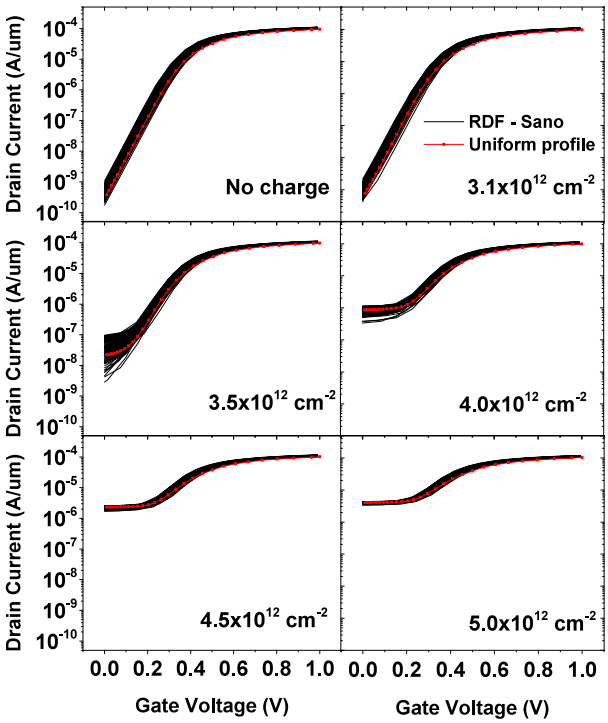

Figure 14: RDF I_d-V_g results of 45nm PDSOI MOSFET. Fixed oxide charge is included in both the BOX and STI. Shown in red is the device with uniform doping profile.

It is also observed that the nominal device shows lower values than the mean. This could potentially be a result of the V_t lowering of the parasitic transistor caused due to randomizing

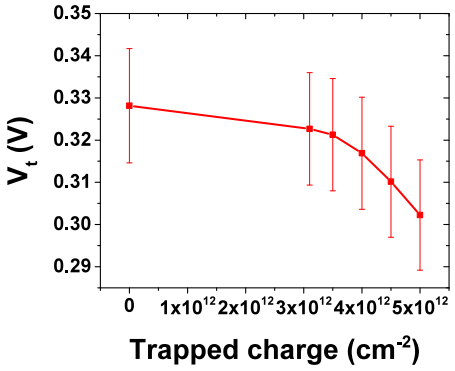

Figure 15: Average and standard deviation of the threshold voltage of the front gate transistor as a function of trapped charge.

the position and number of the dopant atoms. The electrons can thus find the easiest routes through the channel [40]. The tail in the distribution of the count of devices with dopant atoms within a specific range (Figure 13) is directly translated to the devices showing the highest resistance to TID during parasitic channel inversion. σV_t remains constant for all cases of oxide charge examined, as shown in Figure 15.

4.2. Impedance Field Method

RDFs are also examined using the IFM in Sentaurus device. This method uses only one solution to a reference device, and then calculates the effect of the variation as a linear response to a perturbation of the contact characteristics. The Green's function is solved once, for the reference device, for each contact. For the case of contact current, the perturbation due to RDFs at location x will result in the following response,

$$\delta I_c = \int G(x)\,\delta N_\xi(x)\,dx \tag{3}$$

where the integral is for the whole device, c is the contact node, G(x) is Green's function and N_ξ is the equation that involves the doping concentration term [41, 42]. Using a Poisson distribution, the probability to find k dopant atoms in a box volume V_i (cm^{-3}) with average doping concentration N_i (cm^{-3}) at a vertex i of the mesh is,

$$P_i(k) = \frac{(N_i V_i)^k}{k!} exp(-N_i V_i) \tag{4}$$

Both donor and acceptor atoms are taken into account and are treated as separate, uncorrelated sources of variation.

The linear current response δI_d is linked to the nodal drain current dI_d and the gate voltage dV_d variations through the boundary condition,

$$dI_d = \delta I_d + y_{d,g} dV_g \tag{5}$$

where,

$$y_{d,g} = \frac{\partial I_{ref,d}}{\partial V_g} \tag{6}$$

and $I_{ref,d}$ is the drain current of the reference device.

There are numerous techniques for extracting the I_d - V_g characteristics of the randomized profile devices produced with the IFM. These techniques are appropriate either for the on state of the transistor, weak inversion or leakage current. None of them, however, completely covers the situations examined in this work. Namely, it is not just the state of the front gate transistor that is recorded in the I_d-V_g results, but also the state of the parasitic transistor.

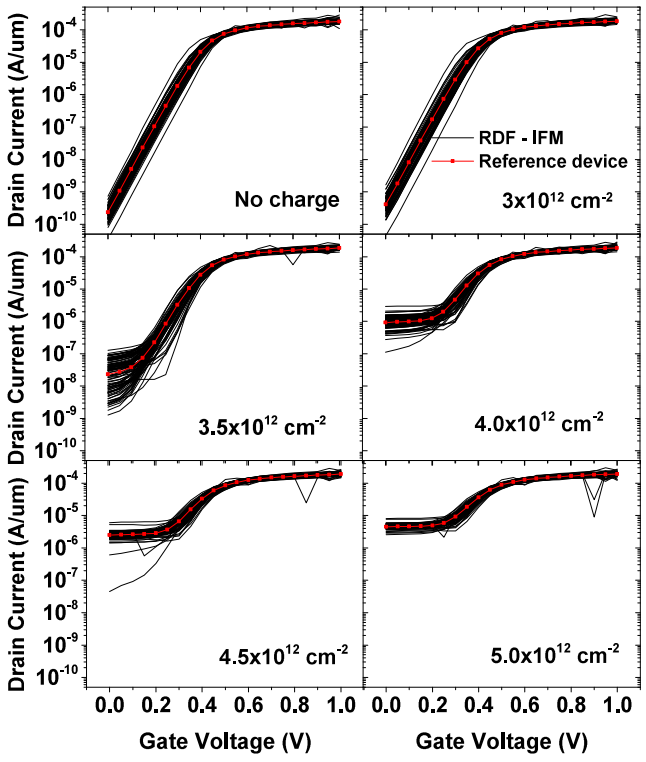

Figure 16: RDF I_d-V_g results using the IFM. Fixed oxide charge is included in both the BOX and STI. Shown in red is the reference device.

In order to take both into account, two methods were used for I_d-V_g extraction. The 'exp' method was used in the cases where the parasitic transistor is off. The drain current in this case is given by,

$$I_{v,d} = I_{ref,d} exp\left(\frac{dI_{v,d}}{I_{ref,d}}\right) \tag{7}$$

and is appropriate only for transistor leakage current. This is due to the breaking of the linearity assumption that results in non-Gaussian distribution in other bias regimes. Therefore, the 'dI' method is used for the cases where the parasitic transistor is in the weak inversion or the on state. This is given by,

$$I_{v,d} = I_{ref,d}\left(V_{ref,g}\right) + dI_{v,d} \tag{8}$$

For the cases where non-physical, negative results occurred during the parasitic channel weak inversion, the 'exp' method was used to represent those specific I_d-V_g results.

The final characteristics of the randomized profile devices are shown in Figure 16. Up to oxide charges of 3.0×10^{12} cm^{-2}, the 'exp' method is used, while the 'dI' method is used for the remaining charges examined. The trends are similar to those in the results of the Sano method with the randomized profile devices exhibiting higher I_{off} spread as we approach the parasitic channel weak inversion and then reducing as the parasitic channel is completely turned on. The artefacts in the saturation region are due to the extraction method chosen.

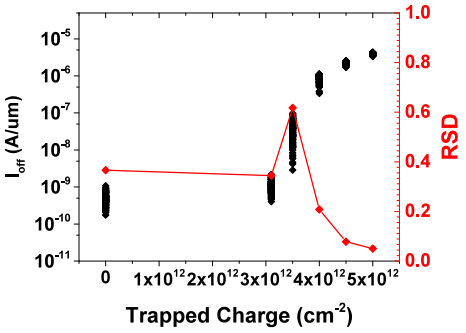

(a) Sano method

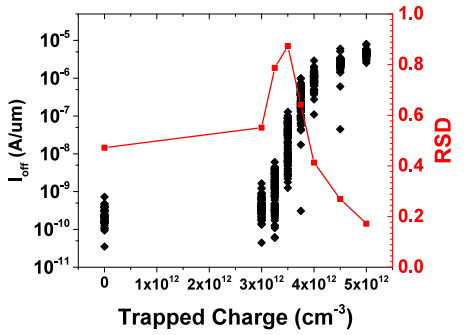

(b) IFM

Figure 17: Relative standard deviation and I_{off} of devices with randomized doping profiles using (a) the Sano method and (b) the IFM.

A comparison between the two randomization methods is shown in Figure 17. The relative standard deviation (RSD) in this figure is the ratio of the standard deviation of I_{off} to the mean. The trend is for RSD to increase until the areal charge of 3.5×10^{12} cm^{-2} (parasitic transistor weak inversion) and then reach practically zero towards 5.0×10^{12} cm^{-2} (parasitic transistor saturation). The two methods are in good agreement, with the IFM producing slightly higher spread in I_{off} values.

RDF results of the device for the case that radiation has created interface traps are shown in Figure 18. The randomized doping profile devices were constructed using the IFM. The densities and activation energies of the traps were chosen so as the highest contribution to I_{off} occurs. The results are similar to the case where radiation has created no interface traps. The parasitic transistor weak inversion now occurs at a lower value of areal charge (3.0×10^{12} cm^{-2}). This is due to the added effect of the interface traps.

Overall, RDFs have reduced the TID hardness of the device

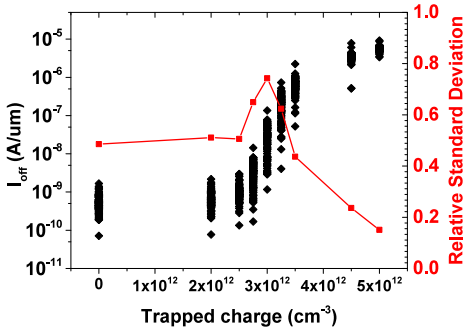

Figure 18: Relative standard deviation and I_{off} of devices with randomized profile using the IFM and interface donor traps of concentration p_{it} = 10^{13} cm^{-2}, E_t = 0.45 eV. The x axis indicates bulk oxide areal charge concentration.

by increasing I_{off} values and are virtually negligible when the parasitic transistor is completely turned on.

5. Conclusions

The combined effects of Total Ionizing Dose and Random Dopant Fluctuations have been examined in the 45 nm PDSOI nMOSFET node. The post-irradiation device response is primarily dictated by the electric field at the bottom silicon corner, even in the case where there in no contact of the S/D junctions to the BOX. The existence of the bottom corner parasitic conduction channel is confirmed with transient radiation simulations where it is shown that the majority of the holes are trapped around the silicon film, creating the effect of lateral gates in the PDSOI nMOSFET.

However, radiation simulations also show that the areal trapped charge required to invert the parasitic transistor is not reached even at a total dose of 600 KRad(SiO_2) and a total trap density of 5×10^{18} cm^{-3}. A threshold was also observed for the charge trapped close to the silicon film as holes trapped there create an electrostatic fence that prevents further movement of holes towards that direction. Donor traps introduced at the silicon interface with the BOX and STI further increased I_{off}, mostly during the parasitic transistor weak inversion.

RDFs create significant response deviation but only in post-irradiation results. In pre-irradiation, the contribution of RDFs is minimal. The post-irradiation device response can deviate significantly, and therefore a greater number of measurements needs to be taken to account for the statistical error. RDFs, generally, aggravate post-irradiation response decreasing the dose level at which the device is hardened against. However, the effect is also more pronounced during weak inversion of the parasitic transistor.

Acknowledgments

The authors acknowledge the support of the UK Engineering and Physical Sciences Research Council (EPSRC) award No. 1304067 as well as the use of the IRIDIS High Performance Computing Facility, and associated services at the University of Southampton.

Data published in this paper are available from the University of Southampton repository at http://eprints.soton.ac.uk/id/eprint/403024.

References

[1] S. T. Liu, A. Hurst, H. L. Hughes, P. Mcmarr, J. Benedito, C. Capasso, Total dose radiation response of a 45nm SOI Technology, IEEE International SOI Conference (2010) 5–6.

[2] N. Rezzak, P. Maillard, R. D. Schrimpf, M. L. Alles, D. M. Fleetwood, Y. A. Li, The impact of device width on the variability of post-irradiation leakage currents in 90 and 65nm CMOS technologies, Microelectronics Reliability 52 (11) (2012) 2521–2526. doi:10.1016/j.microrel.2012.05.013.

[3] D. Mayer, Modes of operation and radiation sensitivity of ultrathin SOI transistors, IEEE Transactions on Electron Devices 31 (5) (1990) 1280–1288.

[4] J. Schwank, Advantages and limitations of silicon-on-insulator technology in radiation environments, Microelectronic Engineering 36 (1-4) (1997) 335–342. doi:10.1016/S0167-9317(97)00076-2.

[5] I. S. Esqueda, H. J. Barnaby, S. Member, M. L. Alles, Two-Dimensional Methodology for Modeling in CMOS Technologies (December) (2005) 2259–2264.

[6] A. Madan, R. Verma, R. Arora, E. P. Wilcox, J. D. Cressler, P. W. Marshall, R. D. Schrimpf, P. F. Cheng, L. Y. Del Castillo, Q. Liang, G. Freeman, The enhanced role of shallow-trench isolation in ionizing radiation damage of 65 nm RF-CMOS on SOI, in: IEEE Transactions on Nuclear Science, Vol. 56, 2009, pp. 3256–3261. doi:10.1109/TNS.2009.2033998.

[7] N. Rezzak, E. X. Zhang, M. L. Alles, R. D. Schrimpf, H. Hughes, Total-ionizing-dose radiation response of partially-depleted SOI devices, 2010 IEEE International SOI Conference (SOI) (2010) 1–2doi:10.1109/SOI.2010.5641057.

[8] N. Rezzak, E. Zhang, D. Ball, Total-ionizing-dose radiation response of 32 nm partially and 45 nm fully-depleted SOI devices, IEEE International SOI Conference (2012) 31–32.

[9] I. S. Esqueda, H. J. Barnaby, K. E. Holbert, F. El-mamouni, R. D. Schrimpf, Modeling of Ionizing Radiation-Induced Degradation in Multiple Gate Field Effect Transistors, IEEE Transactions on Nuclear Science (April) (2011) 499–505.

[10] F. E. Mamouni, S. K. Dixit, R. D. Schrimpf, P. C. Adell, I. S. Esqueda, M. L. Mclain, H. J. Barnaby, S. Cristoloveanu, W. Xiong, Gate-Length and Drain-Bias Dependence of Band-to-Band Tunneling-Induced Drain Leakage in Irradiated Fully Depleted SOI Devices, IEEE Transactions on Nuclear Science (December) (2008) 3259–3264.

[11] R. Schrimpf, D. Fleetwood, M. Alles, R. Reed, G. Lucovsky, S. Pantelides, Radiation effects in new materials for nanodevices, Microelectronic Engineering 88 (7) (2011) 1259–1264. doi:10.1016/j.mee.2011.03.117.

[12] H. Barnaby, M. McLain, I. Esqueda, X. J. Chen, Modeling Ionizing Radiation Effects in Solid State Materials and CMOS Devices, IEEE Transactions on Circuits and Systems I: Regular Papers 56 (August) (2009) 1870–1883. doi:10.1109/TCSI.2009.2028411.

[13] B. Ning, D. Bi, H. Huang, Z. Zhang, Z. Hu, M. Chen, S. Zou, Bias dependence of TID radiation responses of 0.13μm partially depleted SOI NMOSFETs, Microelectronics Reliability (2012) 1–6doi:10.1016/j.microrel.2012.08.005.

[14] P. C. Adell, H. J. Barnaby, R. D. Schrimpf, Band-to-Band Tunneling (BBT) Induced Leakage Current Enhancement in Irradiated Fully Depleted SOI Devices, IEEE Transactions on Nuclear Science 54 (January 2016) (2008) 2174–2180. doi:10.1109/TNS.2007.911419.

[15] N. Rezzak, E. Zhang, D. Ball, Total-ionizing-dose radiation response of 32 nm partially and 45 nm fully-depleted SOI devices, IEEE International SOI Conference (2012) 31–32.

[16] N. Rezzak, R. Schrimpf, Layout-related stress effects on radiation-induced leakage current, IEEE Transaction on Nuclear Science (December) (2010) 3288–3292.

[17] F. T. Brady, J. D. Maimon, M. J. Hurt, A scaleable, radiation hardened shallow trench isolation, IEEE Transactions on Nuclear Science 46 (6) (1999) 1836–1840. doi:10.1109/23.819162.

[18] A. R. Brown, V. Huard, A. Asenov, S. Member, Statistical Simulation of Progressive NBTI Degradation in a 45-nm Technology pMOSFET (September) (2010) 2320–2323.

[19] M. Bukhori, S. Roy, A. Asenov, Simulation of statistical aspects of charge trapping and related degradation in bulk MOSFETs in the presence of random discrete dopants, IEEE Transactions on Electron Devices 57 (4) (2010) 795–803.

[20] S. Narasimha et al., High Performance 45-nm SOI Technology with Enhanced Strain, Porous Low-k BEOL, and Immersion Lithography, 2006 International Electron Devices Meeting (2006) 1–4doi:10.1109/IEDM.2006.346879.

[21] H. S. Yang et al, Dual stress liner for high performance sub-45nm gate length SOI CMOS manufacturing, Applied Physics Letters 75 (2004) 1075–1077. doi:10.1109/IEDM.2004.1419385.

[22] synopsys Inc., Sentaurus Technology Template : 32-nm Gate-First Flow and CMOS Processing.

[23] M. Chudzik et al., High-Performance High- K / Metal Gates for 45nm CMOS and Beyond with Gate-First Processing, IEEE Symposium on VLSI Technology (2007) 194–195doi:10.1109/VLSIT.2007.4339689.

[24] A. Johnston, Low dose rate effects in shallow trench isolation regions, IEEE Transactions on Nuclear Science (December) (2010) 3279–3287.

[25] N. Rezzak, M. L. Alles, R. D. Schrimpf, S. Kalemeris, L. W. Massengill, J. Sochacki, H. J. Barnaby, The sensitivity of radiation-induced leakage to STI topology and sidewall doping, Microelectronics Reliability 51 (5) (2011) 889–894. doi:10.1016/j.microrel.2010.12.013.

[26] F. Brady, H. Hughes, Total dose hardening of SIMOX buried oxides for fully depleted devices in rad-tolerant applications, IEEE Transactions on Nuclear Science 43 (6) (1996) 2646–2650.

[27] M. Turowski, Nonuniform total-dose-induced charge distribution in shallow-trench isolation oxides, IEEE Transaction on Nuclear Science 51 (6) (2004) 3166–3171.

[28] C. Peng, Z. Hu, Z. Zhang, H. Huang, B. Ning, D. Bi, Total ionizing dose effect in 0.2μm PDSOI NMOSFETs with shallow trench isolation, Microelectronics Reliability 54 (4) (2014) 730–737. doi:10.1016/j.microrel.2013.12.016.

[29] A. Johnston, R. Swimm, Total dose effects in CMOS trench isolation regions, IEEE Transactions on Nuclear Science (August) (2009) 1941–1949.

[30] G. I. Zebrev, M. S. Gorbunov, V. E. Shunkov, P. N. Osipenko, B. V. Vasilegin, A. V. Sogoyan, Physical Modeling and Circuit Simulation of Hardness of SOI Transistors and Circuits for Space Applications.

[31] M. L. Alles, H. L. Hughes, D. R. Ball, P. J. McMarr, R. D. Schrimpf, Total-ionizing-dose response of narrow, long channel 45 nm PDSOI transistors, IEEE Transactions on Nuclear Science 61 (6) (2014) 2945–2950. doi:10.1109/TNS.2014.2366725.

[32] S. T. Pantelides, Z. Y. Lu, C. Nicklaw, T. Bakos, S. N. Rashkeev, D. M. Fleetwood, R. D. Schrimpf, The E center and oxygen vacancies in SiO2, Journal of Non-Crystalline Solids 354 (2008) (2008) 217–223. doi:10.1016/j.jnoncrysol.2007.08.080.

[33] S. Pantelides, S. Rashkeev, R. Buczko, D. Fleetwood, R. Schrimpf, Reactions of hydrogen with Si-SiO/sub 2/ interfaces, IEEE Transactions on Nuclear Science 47 (6) (2000) 2262–2268. doi:10.1109/23.903763.

[34] E. Chatzikyriakou, K. Morgan, P. Ashburn, W. Redman-White, C. H. De Groot, Total Ionizing Dose and random dopant fluctuation effects in 65-nm gate length partially depleted Silicon-on-Insulator nMOSFETs, IEEE-NANO 2015 2 (2016) 659–662. doi:10.1109/NANO.2015.7388691.

[35] V. Ferlet-Cavrois, T. Colladant, P. Paillet, J. Leray, O. Musseau, J. Schwank, M. Shaneyfelt, J. Pelloie, J. du Port de Poncharra, Worst-case bias during total dose irradiation of SOI transistors, IEEE Transactions on Nuclear Science 47 (6) (2000) 2183–2188. doi:10.1109/23.903751.

[36] M. Gaillardin, M. Martinez, P. Paillet, F. Andrieu, S. Girard, M. Raine, C. Marcandella, O. Duhamel, N. Richard, O. Faynot, Impact of SOI substrate on the radiation response of ultra thin transistors down to the 20 nm node, IEEE Transactions on Nuclear Science 60 (4) (2013) 2583–2589. doi:10.1109/TNS.2013.2249093.

[37] J. Leray, Total Dose Effects: Modeling for present and future, in: IEEE Nuclear and Space Radiation Effects Conference Short Course, IEEE publishing, Norfolk Virginia, 1999, Ch. III, pp. III–1 – III–4.

[38] N. Sano, K. Matsuzawa, Role of long-range and short-range Coulomb potentials in threshold characteristics under discrete dopants in sub-0.1 μm Si-MOSFETs, IEEE Electron Devices Meeting 2000 (2000) 275–278.

[39] N. Sano, K. Matsuzawa, M. Mukai, N. Nakayama, On discrete random dopant modeling in drift-diffusion simulations: physical meaning of 'atomistic' dopants, Microelectronics Reliability 42 (2) (2002) 189–199. doi:10.1016/S0026-2714(01)00138-X.

[40] a. Asenov, Random dopant induced threshold voltage lowering and fluctuations in sub-0.1 μm MOSFET's: A 3-D "atomistic" simulation study, IEEE Transactions on Electron Devices 45 (12) (1998) 2505–2513. doi:10.1109/16.735728.

[41] A. Wettstein, O. Penzin, E. Lyumkis, W. Fichtner, Random dopant fluctuation modelling with the impedance field method, International Conference on Simulation of Semiconductor Processes and Devices, SISPAD 2003-Janua (October 2003) (2003) 91–94. doi:10.1109/SISPAD.2003.1233645.

[42] K. El Sayed, A. Wettstein, S. D. Simeonov, E. Lyumkis, B. Polsky, Investigation of the statistical variability of static noise margins of SRAM cells using the statistical impedance field method, IEEE Transactions on Electron Devices 59 (6) (2012) 1738–1744. doi:10.1109/TED.2012.2189860.